POLITECNICO
MILANO 1863

DIPARTIMENTO DI MECCANICA

mecc

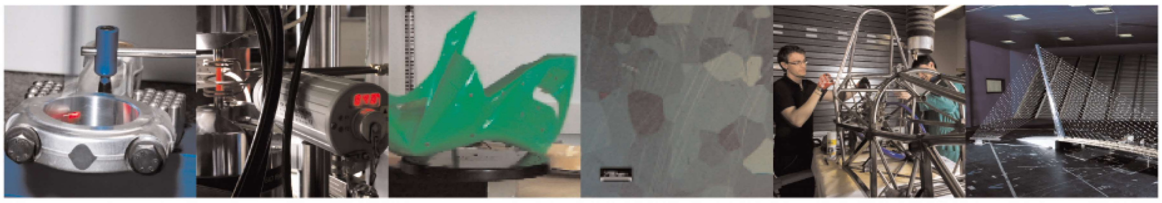

A Meta-Heuristic Optimization Procedure for the Identification of the Nonlinear Model Parameters of Hydraulic Dampers Based on Experimental Dataset of Real Working Conditions

G. Isacchi, F. Ripamonti, M. Corsi

This is a post-peer-review, pre-copyedit version of an article published in Journal of Computational and Nonlinear Dynamics. The final authenticated version is available online at: *https://doi.org/10.1115/1.4062541.*

DIPARTIMENTO DI MECCANICA ■ POLITECNICO DI MILANO
via G. La Masa, 1 ■ 20156 Milano ■ EMAIL (PEC): pecmecc@cert.polimi.it
http://www.mecc.polimi.it
Rev. 0

A meta-heuristic optimization procedure for the identification of the nonlinear model parameters of hydraulic dampers based on experimental dataset of real working conditions

Gioele Isacchi, first author
Politecnico di Milano, Department of Mechanical Engineering
Piazza Leonardo da Vinci, 32 20133 Milan, Italy
Gioele.isacchi@polimi.it

Francesco Ripamonti, second author
Politecnico di Milano, Department of Mechanical Engineering
Piazza Leonardo da Vinci, 32 20133 Milan, Italy
francesco.ripamonti@polimi.it

Matteo Corsi, third author
KONI BV,
Korteweg 2, 3261 NH Oud-Beijerland, Netherlands
Matteo.corsi@itt.com

ABSTRACT

Hydraulic dampers are widely implemented in railway vehicle suspension stages, especially in high-speed passenger trains. They are designed to be mounted in different positions to improve comfort, stability, and safety performances. Numerical simulations are often used to assist the design and optimization of these components. Unfortunately, hydraulic dampers are highly nonlinear due to the complex fluid dynamic phenomena taking place inside the chambers and through the by-pass orifices. This requires accurate damper models to be developed to estimate the influence of the nonlinearities of such components during the dynamic performances of the whole vehicle. This work aims at presenting a new parametric damper model based on a nonlinear lumped element approach. Moreover, a new model tuning procedure will be *introduced. Differently from the typical sinusoidal characterization cycles, this routine is based on experimental tests of real working conditions. The set of optimal model parameters will be found through a meta-heuristic iterative approach able to minimize the differences between numerical and experimental damper forces. The performances of the optimal model will be compared with the ones of the most common Maxwell model generally implemented in railway multibody software programs.*

1 INTRODUCTION

Hydraulic dampers are one of the most diffused types of suspension components in railway vehicles. The hydraulic dampers are characterized by a dissipative effect caused by the liquid flowing through the internal orifices of the component. Dampers are generally implemented in both primary and secondary suspension stages of passenger vehicles [1] and are oriented in different directions. Different experimental approaches have been developed to support the design of new suspension components, such as field tests or Hardware-In-the-Loop (HIL) simulations. The HIL experimental technique has been adopted in many works to investigate the performances of prototype suspensions [2] due to its lower cost respect to field tests.

Nowadays, in order to further reduce the design cost, the development of new hydraulic dampers for railway vehicles is largely supported by virtual simulations and laboratory experimental tests. These procedures aim at evaluating the effects of the studied component on the dynamic performances of the vehicles. In railway engineering, the virtual simulations are generally based on the multibody approach, which allows to represent the dynamic coupling between the vehicle subsystems (wheelsets, bogies, carbodies, etc.) through the implementation of several suspension elements. The multibody approach proved to be very effective in simulating the dynamics of railway vehicles, but, according to Evans and Berg [3] and Bruni et al. [4], there are still several challenges, especially in implementing the correct modelling approach of the different suspension components.

The modelling of hydraulic dampers through accurate virtual models is fundamental to obtain reliable numerical results. The damper numerical models must be simple and fast in order to reduce the computational effort of multibody analysis, especially considering that a railway vehicle contains a large amount of suspension components to be modelled. Moreover, the use of damper models with low computational effort is a requirement for the design of vehicle models able to be run in real time during HIL tests. For these reasons it is important to obtain the maximum accuracy from simple suspension models before considering switching to more complex approaches.

The dynamics of hydraulic dampers is not trivial due to their nonlinear nature. For instance, in the most common solution, the damping force, strongly related to the damper elongation speed, is limited by a blow-off valve which avoids extreme force development. Furthermore, railway dampers present an asymmetric behavior between rebound and compression strokes. Asymmetry is generally more relevant in vertical devices [5]. The damper modelling approach cannot exempt from considering also that the dynamic behavior of the component is strongly influenced by its overall flexibility. Indeed, hydraulic dampers are not purely dissipating elements. Oil compressibility, elasticity of piston and cylinder are the most important contributions to the device flexibility. Moreover, the presence of resilient rubber mounts at the damper-vehicle interfaces, also known as silent blocks, increases the complexity of the system due to their nonlinear elastic and dissipating contributions. Several studies investigated the relevance of a correct damper flexibility modelling. For example, according to [4, 6, 7, 8], the influence of the yaw damper flexibility is fundamental to correctly estimate the stability of railway vehicles. Stability assessments performed without considering an in-series stiffness tends to overestimate the performances of the vehicle [6, 8]. According to [9, 10], an accurate modelling of the yaw damper is crucial to assess the vehicle dynamics. The correct estimation of the damper stiffness is also important in the evaluation of ride comfort performances: different studies [11, 12, 13] considered this effect when modelling yaw or vertical dampers.

In this context, this work aims at introducing a damper model based on lumped parameters able to represent the nonlinear dynamics of a physical damper prototype. This model has been developed in Simulink to be co-simulated with a vehicle model in multibody environment and to be implemented in real time on a HIL test bench. Together with the parametric model, an optimal identification procedure is presented. Previous works focused applied Genetic Algorithm or Particle Swarm Optimization [14, 15, 16] to tune lumped element models on real damper prototypes by comparing numerical and experimental forces obtained by applying sinusoidal characterization cycles. Moreover, large attention has been given to the application of optimal identification procedures to numerical models representing magnetorheological dampers. Rodríguez-Torres et al. [17] tuned nonlinear models for benchmark purposes by considering Genetic Algorithm and Particle Swarm Optimization. Several works focused their attention on the identification of the best parameters of Bouc-Wen model for calculating the force provided by magnetorheological dampers [18, 19, 20]. Differently from the previous works, this paper applies the meta-heuristic Firefly algorithm [21] to identify the optimal parameters of the proposed damper model. This paper focuses its attention on hydraulic dampers, widely adopted on railway vehicles. This approach has been designed to optimize an objective function by simulating the evolution of a set of candidates (in this case, several numerical damper models). This iterative method can identify the set of parameters able to optimize the accuracy of the damper model. Differently from the previously works, the procedure proposed in this paper is based on a set of experimental tests which are similar to the strokes imposed on railway dampers during the real operating conditions of the vehicles. This approach differs from the use of simple sinusoidal cycles. Indeed, differently from the typical sinusoidal tests this approach aims at introducing a tuning of the damper model based on the experimental reproduction of real maneuvers. The real scenarios will be first simulated with a multibody vehicle model to obtain the significative strokes able to characterize the damper in typical conditions (curved or straight track negotiation). Then, an experimental test rig will impose these reference strokes on the real damper and will measure the force provided by the prototype. The optimization procedure will compute the set of model parameters able to minimize the difference between the measured damper forces and virtual forces provided by the damper model during the different operating conditions.

This paper is organized as follows: section 2 will introduce the damper parametric model together with the tuning procedure and the experimental setup to evaluate the benchmark damper forces. Moreover, the parameter identification procedure will be presented. Section 3 will report the performances of the optimal damper model and will compare it against a linear Maxwell model, a common damper modelling approach found in railway dynamics. Section 4 will discuss and conclude the paper.

2 MATERIALS, METHODS AND MODELS

2.1 Damper model

This work introduces a damper model that aims at reproducing the dynamics of a generic passive hydraulic damper. The lumped elements approach has been chosen to design the model. This choice reduces the computational effort required, making it compatible with multibody vehicle simulations and real time procedures, such as HIL approach.

In railway dynamics, numerical simulations require to properly model the components of the vehicle suspension stages according to a trade-off based on model accuracy and computational time. The linear dashpot is the simplest modelling approach for a generic damper. As a matter of fact, this single element can not represent the complex dynamic of a shock absorber. Indeed, despite dampers are generally defined as purely dissipative elements, their behavior is also related to an elastic contribution. The damper virtual model proposed in this paper is reported in figure 1. The model describes the effects of the silent blocks by means of two sub-models composed by parallel linear terms, k_B and c_B. They represent respectively the elastic and dissipative actions of the resilient silent blocks. Between the two silent blocks, a main sub-model is inserted to simulate the damper structure. In this sub model, three mass elements M_C, M_O and M_P are introduced to account for the inertial terms. Generally, such elements are neglected in the lumped parameters damper modelling [12]. Nevertheless, they are introduced here to allow the general damper model to simulate device layouts characterized by very soft damping action where the inertial terms become more relevant. Between the mass element, two nonlinear forces are inserted. The $F_{k,O}$ force is introduced to model the elastic contribution, related to both oil compressibility and internal structure flexibility. The second force $F_{c,O}$ aims at describing the nonlinear dissipative action due to the oil flow through the piston orifices.

The dynamics of the damper model is described by a set of ordinary differential equations (ODEs):

$$M_C\ddot{x}_4 + k_B x_4 + c_B\dot{x}_4 + F_{k,O} = 0 \quad (1)$$

$$M_O\ddot{x}_3 + F_{k,O} + F_{c,O} = 0 \quad (2)$$

$$M_P\ddot{x}_2 + F_{c,O} + k_B(x_2 - x_1) + c_B(\dot{x}_2 - \dot{x}_1) = 0 \quad (3)$$

$$F = c_B(\dot{x}_2 - \dot{x}_1) + k_B(x_2 - x_1) \quad (4)$$

derived by imposing the equilibrium conditions to the elements of the system. The presence of $F_{k,O}$ and $F_{c,O}$, which are respectively a function of the relative displacement $(x_4 - x_3)$ and of the relative speed $(\dot{x}_3 - \dot{x}_2)$, makes the system strongly nonlinear [22]. Moreover, these parameters are designed to be asymmetric to represent the differences between compression and rebound strokes. This property is particularly relevant both in stability [23] and in ride comfort evaluations [5].

2.2 Experimental tests based on numerical simulations

In this work, we focused our attention on a yaw damper prototype (twin-tube, spool-valves Type 06, manufactured by Koni). The choice of a yaw damper has been made considering that such devices are the most challenging dampers to be modelled in railway dynamics. The virtual model must accurately reproduce the force of the damper prototype. For this reason, experimental tests are performed to measure the benchmark damper force to be used in the tuning of the parametric damper model.

Dampers for rail vehicles are typically characterized by imposing sinusoidal cycles with stroke, speed, and frequency defined according to the EN 13802 standard. Nevertheless, sinusoidal displacements are far away from the working conditions experienced in real operating scenarios. Indeed, it is important to consider that tuning a parametric virtual model on experimental data representing unrealistic conditions might reduce the capability of the model to accurately reproduce the damper dynamics during real maneuvers. For this reason, in the tuning procedure proposed in this paper, experimental force signals have been obtained by imposing on the damper prototype a set of displacement time histories able to emulate the working conditions of the damper. The damper forces obtained from the prototype will also be considered as benchmark to evaluate the accuracy of the virtual damper model.

Figure 2 shows the block diagram of the overall tuning procedure, divided into the upper identification branch and the lower validations stage. The damper strokes during the vehicle maneuvers have been obtained through a single-wagon multibody model developed with the Simpack software. The model is composed of seven rigid bodies: a carbody, two bogies, and four wheelsets. The simulated vehicle represents a generic high-speed train. Besides the four nonlinear yaw dampers, the suspension components have been modelled with a linear approach. The reference damper strokes have been obtained from the front-right yaw damper. The damper stroke time histories are then imposed on the damper prototype to obtain a set of experimental reference force signals ($F_{Exp,Id}$ and $F_{Exp,Val}$). For each experiment, one of the reference strokes obtained by the multibody model is imposed on the damper prototype through a servo-controlled MTS® actuator (MTS, Type 248.05, rating force: 50 kN), managed by a SpeedGoat® Real Time Computer. The damper force provided by the prototype is measured by a load cell (Hottinger Baldwin Messtechnik, Type U10M/50, sensitivity 2.1021 mV/V, adjusted range 50 kN). Figure 3 shows the experimental test bench with the MTS® Control Unit and the SpeedGoat Real Time Computer.

The experimental damper forces of the identification scenarios ($F_{Exp,Id}$) are used as a benchmark for the identification of the optimal parameters of the damper model, while the force signals obtained from the tuned damper model simulating the validation scenarios ($F_{Num,Val}$) are compared to their experimental equivalent ($F_{Exp,Val}$) to estimate the accuracy of the tuned damper model.

In the identification scenario we simulated three different maneuvers to obtain the reference strokes. The first two scenarios are characterized by track irregularity profiles defined stochastically considering the superimposition of harmonics with wavelengths between [3 m, 200 m]. The harmonics are characterized by random phases and deterministic magnitude obtained from the analytical Power Spectral Density (PSD) functions able to replicate the typical frequency contents of a track irregularity, according to [1, 24]. The polynomial formulation of the track irregularity PSD is implemented according to the report B176 of the European Rail Research Institute [25]. The three identification scenarios describe:

- Identification 1: a straight track running in high-speed condition: this test aims at simulating the vehicle dynamics at speed equal to 250 km/h, with track irregularity.
- Identification 2: a low-speed negotiation of a sharp curve: the railway vehicle simulates the negotiation of a curved track segment composed by a transient curve entry, a constant curvature segment and a transient curve exit, with track irregularity. The curve radius is 400 m. The track has been negotiated at 72 km/h.
- Identification 3: a very low-speed negotiation of a switch: the test is based on the S-curve maneuver reported in Annex F of EN 14363. The vehicle speed is set at 43 km/h.

The reference damper strokes obtained from the multibody model running the identification scenarios are reported in figure 4.

The selection of the three different scenarios aims at representing the most important working conditions related to the prototype under investigation (a yaw damper). The straight running in high-speed conditions is characterized by high frequency oscillations with small amplitudes. In this condition, the yaw dampers are expected to improve the stability by suppressing the tendency of the vehicle to show hunting motion [6]. In the negotiation of the curved track, at the constant curvature gradient of the curve entry, an exit transient can be observed, together with the constant curvature track segment. Here, yaw dampers provide a negative steering resistance effect which is responsible for a deterioration of the curving performances of the vehicle [26]. This negative effect is further amplified during the negotiation of switches or crossing [13], as shown by the last scenario. The negotiation of the switch is an interesting condition due to the low-frequency high-amplitude displacement imposed on the yaw dampers. The damper dynamics in these conditions is significantly different from the high-frequency low-amplitude oscillations of high-speed running [27].

Beside the identification scenarios, a second set of maneuvers, known as validation, is defined with the aim of verifying in different conditions the accuracy of the damper model tuned by the optimization procedure. The track irregularities of the validation scenarios are described obtaining new profiles characterized by harmonics with magnitude obtained from the same PSD analytical description reported in [25] but with different random phases. This approach generates irregularity signals that are different between identification and validation scenarios but with frequency contents that are aligned to the ones observed in real rail tracks. The validation scenarios can be listed as:

- Validation 1: a straight track running in high-speed condition. This test aims at simulating the vehicle dynamics at speed equal to 250 km/h, with a different track irregularity profile with respect to the identification scenario 1.
- Validation 2: a high-speed negotiation of a large radius curve with track irregularity. The curve radius is set equal to 6000 m, while the vehicle speed is 306 km/h.
- Validation 3: a low-speed negotiation of a sharp curve. The railway vehicle simulates the negotiation of a curved track segment composed by a transient curve entry, a constant curvature segment and a transient curve exit. The curve radius is 500 m. The track is negotiated at 86 km/h and track irregularity is implemented.

The damper strokes of the validation scenarios are reported in figure 5. The identification and validation scenarios are summarized in table 1.

This procedure allows the definition of a set of experimental time histories of the damper force starting from the damper strokes obtained in the multibody analysis. It is worth remarking that the approach can be generalized and implemented with any kind of suspension component as long as it is possible to develop a multibody model of the vehicle able to simulate the stroke signals of the suspension component of interest in its most typical operating conditions.

2.3 Optimal parameter identification

Objective function

The identification procedure aims at defining the optimal set of model parameters (section 2.1) able to guarantee the best accuracy in modelling the damper force. The experimental procedure illustrated in the previous section gave as results three force measurements related to typical operating conditions: straight track, small radius curve, switch negotiation. The three damper strokes can be imposed on the damper numerical model to simulate the same scenarios in a virtual environment. Therefore, the accuracy of a generic damper model can be evaluated by comparing the virtual force with the experimental benchmark signals. The optimal damper model is then characterized by the set of parameters able to minimize the difference between experimental force measurements and correspondent virtual forces.

Design variables

The set of model parameters represents the design variables of the optimization problem. The damper model described in section 2 has five constant parameters, representing the three masses (M_C, M_O, M_P) and the silent blocks elements (k_B, c_B). Moreover, the highly nonlinear behavior of the damper oil is represented by two variable quantities, $F_{k,O}$, $F_{c,O}$. They represent the nonlinear damping force related to the relative speed $(\dot{x}_3 - \dot{x}_2)$ and a nonlinear elastic force which is a function of the relative displacement $(x_3 - x_4)$. These functions are respectively described by 14 samples in the force-speed diagram and 10 samples in the force-displacement one (piecewise function). The speed and displacement coordinates are set before the optimization procedure considering the typical working range of the damper under analysis. Considering the yaw damper prototype, a higher number of points have been introduced in low relative speed or displacement regions, and a larger refinement has been used in regions with higher relative speed or displacement. The 24 force values, required to fully describe the two nonlinear relationships, are considered as parameters to be identified. Therefore, the optimization problem aims at obtaining 29 modelling parameters.

All the design variables have been constrained. The three concentrated masses have been defined in the range [1 – 20] kg. The bushing properties k_B and c_B, have been respectively constrained between [1e2 – 1e9] N/m and [1e2 – 1e7] Ns/m. The 14 samples illustrating the nonlinear damping effect of the oil have been constrained by applying a limit to the maximum force values obtained from a preliminary quasi-static characterization test, performed on the prototype with sinusoidal mono-harmonic cycles. In this application, the maximum force is set to 3e4 N. The 10 samples related to the nonlinear elastic effect of the oil have been constrained by applying bounds around the expected elastic force of the typical linear spring which is implemented in yaw damper modelling (1.5e7 N/m).

Optimization procedure

The pursuit of the optimal model tuning has been based on a meta-heuristic iterative approach, the Firefly Algorithm (FA). This procedure, presented in [21], was inspired by the capability of fireflies to attract other individuals by producing a bioluminescence from their abdomen. Fireflies with lighter abdomens are more prone to attract other individuals and are characterized by a large fitness. FA starts with an initial population of model candidates which maintains a fixed number of individuals. FA simulates the evolution of the population by modifying their parameters. For each iteration, the less bright candidates (low fitness individuals) are forced to emulate the settings of the shinier candidates (high fitness individuals). The fitness of a model candidate is calculated by imposing the three damper strokes to the model and comparing the provided virtual forces with the measured experimental forces. The experimental damper force F_{Exp} and the numerical force F_{Num} are defined as discrete time series (length N) including the three operating conditions described in section 2. Similarly to [17], the fitness G of a model candidate is calculated according to:

$$G = \frac{N}{\sum_{j=1}^{N} \left(F_{Exp,j} - F_{Num,j} \right)^2} \qquad (\mathbf{5})$$

where the *j* index specifies the time sample of the two force time series, F_{Exp} and F_{Num}. Within each iteration, the FA modifies the parameters of an individual by moving it towards the brighter individuals. Once a i-esimal model candidate is selected, the method updates its 29 parameters of the i-model according to:

$$\check{x}_i^{New} = \check{x}_i + A_{ij} = \check{x}_i + \sum_{j=1}^{M} \left[\frac{G_0}{1 + \varepsilon d_{ij}^2} \left(\check{x}_j - \check{x}_i \right) + \rho R_j \right] \qquad (\mathbf{6})$$

The new vector of scaled design variables $\check{x}_{i,new}$ is obtained starting from the original scaled set $\check{x}_i$, where M is the number of individuals showing a fitness G_j higher than G_i. The design variables have been scaled with respect to their correspondent lower and upper bounds to avoid discrepancies due to different order of magnitude of their scalar values.

The second term of equation 6 describes the attraction A_{ij} of the brighter firefly j on the firefly i. This term forces the parameters of the model i towards the correspondent values of the more accurate model j. The attractiveness coefficient G_0 describes the tendency of the fireflies to be attracted by other brighter individuals. The attractiveness between fireflies is reduced by the relative distance between the two individuals in the design variable domain (d_{ij}). This term is based on the Cartesian distance between the normalized design variables (*p*) of the two models, $\breve{x}_i$ and $\breve{x}_j$:

$$\boldsymbol{d_{ij}} = \sqrt{\sum_{p=1}^{29} \left(\breve{\boldsymbol{x}}_{jp} - \breve{\boldsymbol{x}}_{ip}\right)^2} \qquad (\mathbf{7})$$

The attractiveness is also conditioned by the absorption coefficient ε, which weights the influence of the distance on the attractiveness across different fireflies. A greater value of ε brings to a more relevant reduction of attractiveness at higher distances. The coefficient ε has been set equal to 0.8.

In FA, the modification of the population is also based on a random contribution that influences the variation of the design variables of the individuals. This casual effect allows the iterative method to better explore the domain of the design variables during the search of the optimal solution. Therefore, the random contribution is represented by a 29-dimension vector of random variables (R_j). This vector is calculated for each modification of an i-esimal individual, while the domains of the 29 random terms are restricted according to the vectors L_{Min}, L_{Max}, defining the lower and upper bounds for each p-esimal dimension. These limits are defined as:

$$L_{Min,i} = \begin{bmatrix} -\check{x}_{i,1}^{New} \\ \vdots \\ -\check{x}_{i,p}^{New} \\ \vdots \\ -\check{x}_{i,29}^{New} \end{bmatrix}, L_{Max,i} = \begin{bmatrix} 1-\check{x}_{i,1}^{New} \\ \vdots \\ 1-\check{x}_{i,p}^{New} \\ \vdots \\ 1-\check{x}_{i,29}^{New} \end{bmatrix} \quad (\mathbf{8})$$

The vector R_j is multiplied by an influence coefficient ρ which weights the relevance of the random component on the evolution of the individuals. Random terms are very important in the first stage of the evolution of the population of the damper model. On the other hand, high random contributions reduce the convergence rate of the FA method. For this reason, we introduced a decrement logarithm law to define a variable influence coefficient ρ according to the number of the iteration *k*: $\rho = {\rho_0}^{k-1}$, where ρ_0 coefficient has been set equal to 0.9. This variation aims at preserving the advantages of high random influence in the first iterations without decreasing the capability of the FA procedure to converge in the following iterations.

3 RESULTS AND DISCUSSION

The results are presented in the following two sections. The first will report the optimal set of model parameters obtained from the FA, while the second will show the capability of the optimal damper model to replicate the experimental behavior among a new set of real maneuvers. The performances of the optimal model will be also compared with the ones of a Maxwell linear model. This comparative analysis aims at highlighting the differences between the accuracy of the proposed model and a damper modelling approach widely implemented in railway dynamics. The linear Maxwell model has been tuned with the same iterative procedure presented in section 2.

3.1 Optimal damper model

The FA procedure has been implemented with a population of 20 individuals. Figure 6 shows the progressive increase of the average population fitness (G_{Mean}). The approach simulated the evolution of the population during a maximum of 150 iterations. As we can observe, the algorithm converges towards an optimal solution in the last iterations. However, besides the maximum number of iterations, a further stopping criterion, based on the gradient of the average fitness of the population, is considered starting from the 20th iteration. In particular, the algorithm is designed to stop when the average fitness of the k-esimal population is minor than a threshold defined on the mean of the last 20 average fitness values:

$$stop\ if \quad G_k < 0.001\frac{\sum_{t=k-20}^{k} G_{Mean,t}}{20}$$

During evolution, the individual with the best fitness is always stored to obtain the best model at the end of the procedure. The storing of the overall best candidate avoids excluding eventual optimal solutions found during the initial stages of the procedure, where the strong influence of the random effect could lead to a loss of this candidate.

Figure 7 compares the 5 constant parameters of the initial population (randomly defined) with the ones of the final population. As can be observed, the five parameters (M_C, M_O, M_P, k_B, c_B) are randomly distributed in the initial population but converge to an optimal value in the final population (green markers almost coincident).

Similarly, the nonlinear behavior of the oil is represented in figure 8 by the elastic $F_{k,O}$ and the dissipative $F_{c,O}$ contributions. The two nonlinear relationships are compared for initial and final populations. We can observe how in the final population the curves tend to converge to an optimal nonlinear trend.

In summary, the optimal parameters of the proposed damper model are reported in table 1.

3.2 Performance of the optimal damper model

As a final step the optimal damper model is simulated in real working conditions. The validation scenarios have been used to verify the performances of the optimal model in simulating the dynamics of the physical damper prototype in conditions different with respect to the dataset used during the identification procedure. To quantify the modelling accuracy of the proposed model, a linear Maxwell model has also been tuned with the same procedure. The linear Maxwell model is a common approach when simulating dampers of rail vehicles dampers [4] and it will be assumed as a reference case.

Figure 9 compares the experimental forces obtained from the test rig with the numerical forces obtained by the proposed numerical model and the optimal tuned Maxwell linear model in the 3 validation scenarios.

In figure 9a, the numerical force obtained by the optimal damper model shows a very good correlation with respect to the experimental force during the low-speed negotiation of sharp curves. Moreover, this simulation highlights a typical limitation affecting the linear Maxwell model. Indeed, due to the constant damping ratio of the Maxwell model, the transient curve segments (seconds 2-8 and seconds 13-19) show poor performances. This issue is even more critical considering that the lower damper forces during curve negotiation leads to an overestimation of the curving performance of the vehicle [26]. On the other side, the use of the proposed model allows to significantly reduce the error.

In figures 9b and 9c, high-speed conditions are analyzed. Both straight track and large radius curve show a good correlation between the experimental data and the proposed model. Also in this case, the Maxwell model provides lower damping forces. This would cause a reduction in the dynamic indexes related to the vehicle stability, such as bogie lateral accelerations [13]. The difference between the experimental damper force and the numerical forces obtained with the optimal model are reported in figure 10. The presented results have been quantified in table 2, in which the Mean Squared Error (MSE) and the Absolute Mean Error (AME) between experimental and numerical forces, for both the models and all the simulations, are reported. The MSE and AME formulations reported in table 2 are based on the index i which defines the i-esimal time sample of the two force time histories. The proposed damper model accurately simulates the forces during all the real operating conditions, with a maximum absolute error lower than 2400 N (when a peak force of 18 kN is found at 5.5 s of the second validation test). During negotiation of low radius curves the nonlinear model reduces the error up to 88% with respect to the Maxwell model and an AME with respect to experimental data lower than 350 N is observed. In high-speed conditions the AME rises to 500-550 N but a significant improvement of the nonlinear model with respect to the Maxwell one is still present (-67%).

To better investigate the optimized model, the nonlinear elastic and damping terms $F_{k,O}$ and $F_{c,O}$ reported in table 2 are analyzed in figure 11 with the aim of quantifying their linearity and symmetry. The two terms have been fitted with both a 5th order polynomial and a linear function. The equations of the 5th order polynomial interpolators $F_{kO,5th}$ and $F_{cO,5th}$ are reported:

$$\begin{aligned} F_{kO,5th} = {} & -9.047\mathrm{e}17(x_4 - x_3)^5 + 1.149\mathrm{e}14(x_4 - x_3)^4 + 4.689\mathrm{e}12(x_4 - x_3)^3 \\ & -2.558\mathrm{e}8(x_4 - x_3)^2 + 1.335\mathrm{e}7(x_4 - x_3) + 12.37 \end{aligned} \tag{9}$$

$$\begin{aligned} F_{cO,5th} = {} & 5.932\mathrm{e}10(\dot{x}_3 - \dot{x}_2)^5 + 3.884\mathrm{e}6(\dot{x}_3 - \dot{x}_2)^4 - 6.911\mathrm{e}8(\dot{x}_3 - \dot{x}_2)^3 \\ & -1.170\mathrm{e}5(\dot{x}_3 - \dot{x}_2)^2 + 1.234\mathrm{e}6(\dot{x}_3 - \dot{x}_2) + 57.96 \end{aligned} \tag{10}$$

By comparing the identified nonlinear trends (green lines) with the linear interpolation function (dashed black lines), it can be observed that the damping term $F_{c,O}$ is showing nonlinear behavior more relevant than the elastic term $F_{k,O}$. Nevertheless, by comparing $F_{k,O}$ with the linear function, it is possible to observe its nonlinear trend, especially in the low displacement region (see figure 11c). The 5th order polynomial function is reported in figure 11 by dividing the even order terms (yellow cross) from the odd order terms (red plus). The even order terms can be related to the asymmetry of the nonlinear terms between compression and rebound phases. According to figure 11, it can be stated that the hydraulic damper under investigation presents a symmetric behavior. Indeed, the optimal trends are almost completely defined by the odd order terms of the 5th order polynomial. This last result is aligned to the expectation: the device under investigation is a new yaw damper, designed to provide a symmetric action during both compression and rebound phases.

4 CONCLUSIONS

In this work, a new parametric nonlinear model for hydraulic dampers is proposed. The model, based on a lumped parameter approach, is designed to simulate a generic hydraulic damper in different operating conditions and guarantee good accuracy with reduced computational efforts. The model features two nonlinear terms which aim at representing the intrinsic nonlinear behavior of hydraulic dampers.

The proposed methodology tunes the damper model on a physical prototype of a yaw damper. The training dataset for the model tuning has been obtained with a specific test rig designed to impose on the prototype different strokes and measure the damper force. These target strokes have been obtained from multibody analysis simulating real operating conditions of a high-speed rail vehicle.

The tuning of the damper model has been performed by introducing an iterative optimization procedure based on the meta-heuristic Firefly Algorithm. This routine, focused on the minimization of the differences between virtual and experimental forces, gave as result an optimal set of model parameters.

The performances of the optimal damper model have been compared with a best tuned Maxwell model, a typical damper modelling approach implemented in railway dynamics. The proposed nonlinear model has proved to be able at simulating the damper dynamics in very different conditions, simulating the maneuvers performed by rail vehicles. This model reduced by one order of magnitude the mean squared error of the linear Maxwell models, returning an absolute mean error between numerical and experimental forces below 600 N. Moreover, the optimal nonlinear terms of the damper model have been investigated though the use of polynomial interpolations. A nonlinear behavior has been identified on the dissipative nonlinear term while the elastic term is characterized by a smaller nonlinearity, localized in the low displacement region. This analysis also highlighted the symmetric behavior of the tested damper.

As a conclusion, the nonlinear model proved to be a good solution for the simulation of the dynamics of a real damper prototype in different conditions. The optimal procedure demonstrated to be an interesting approach for optimizing the modelling capabilities of generic dynamic models. The definition of a training dataset based on real operating conditions maximized the capability of the damper model of simulating real working conditions. In suspension modelling the use of the proposed procedure represents a good solution to increase the model accuracy, both in straight track (stability) and curve negotiation (wheel-rail wear) analysis, preserving the computational effort.

FUNDING

The authors received no financial support for the research and/or publication of this article.

NOMENCLATURE

A_{ij}	Attraction of the brighter firefly j on the firefly i
c_B	Linear damping related to the silent block
d	Distance between two fireflies
$F_{c,O}$	Nonlinear damping force acting between elements O, P
$F_{cO,5th}$	Expression of the 5th order polynomial interpolator of $F_{c,O}$
$F_{Exp,Id}$	Time histories of the experimental damper forces measured from the damper prototype during the replication of the identification scenarios on the test bench
$F_{Exp,Val}$	Time histories of the experimental damper forces measured from the damper prototype during the replication of the validation scenarios on the test bench
$F_{k,O}$	Nonlinear elastic force acting between elements C, O
$F_{kO,5th}$	Expression of the 5th order polynomial interpolator of $F_{k,O}$
$F_{Num,Id}$	Time histories of the numerical damper forces obtained from the damper model in the identification scenarios
$F_{Num,Val}$	Time histories of the numerical damper forces measured from the damper prototype during the replication of the identification scenarios on the test bench
G	Fitness of a single damper model candidate

G_0	Attractiveness coefficient
k_B	Linear stiffness related to the silent block
L_{Max}	Design variable upper bound
L_{Min}	Design variable lower bound
M_C	Concentrated mass, element C
M_O	Concentrated mass, element O
M_P	Concentrated mass, element P
R	Random contribution
$x_{1,Id}$	Generic time history of the damper stroke during identification scenarios
$x_{1,Val}$	Generic time history of the damper stroke during validation scenarios
$\breve{x}_i$	Vector of the design variables of the i-esimal damper model candidate scaled on the proposed lower and upper bounds.
ε	Absorption coefficient
ρ	Influence coefficient of the random term

Bibliography

[1] S. Iwnicki, Handbook of Railway Vehicle Dynamics, CRC Press, Taylor & Francis, 2006.

[2] F. Ripamonti and A. Chiarabaglio, “A smart solution for improving ride comfort in high-speed railway vehicles,” *Journal of Vibration and Control,* vol. 25, no. 13, 2019.

[3] J. Evans and M. Berg, “Challenges in simulation of rail vehicle dynamics,” *Vehicle System Dynamics,* vol. 47, no. 8, pp. 1023-1048, 2009.

[4] S. Bruni, J. Vinolas, M. Berg, O. Polach and S. Stichel, “Modelling of suspension components in a rail vehicle dynamics context,” *Vehicle System Dynamics,* vol. 49, no. 7, pp. 1021-1072, 2011.

[5] M. Dumitriu, “Study on the Effect of Damping Asymmetry of the Vertical Suspension on the Railway Bogie Vibrations,” *Symmetry,* vol. 14, no. 2, 2022.

[6] A. Alonso, J. Gimenez and E. Gomez, “Yaw Damper Modelling and its Influence on Railway Dynamic Stability,” *Vehicle System Dynamics,* vol. 49, no. 9, 2011.

[7] M. Wrang, “Instability Phenomena of a Passenger Coach, Caused by Internal Yaw Damper Flexibility,” *Vehicle System Dynamics,* vol. 33, 2000.

[8] C. Huang and J. Zeng, “Comparison of the Maxwell model and a simplified physical model for a railway yaw damper in damping characteristics and vehicle stability assessment,” in *Proceedings of the Institution of Mechanical Engineers Part F Journal of Rail and Rapid Transit*, 2021.

[9] S. Bruni, P. Belforte, A. Cera, H. Hartwig, G. Mancini and L. Mazzola, “Experimental investigation of yaw damper performances: an improved and harmonised testing methodology developed within ModTrain EU project,” in *8th World Congress on Railway Research (WCRR 2008)*, 2008.

[10] O. Polach and I. Kaiser, “Comparison of Methods Analyzing Bifurcation and Hunting of Complex Rail Vehicle Models,” *J. Comput. Nonlinear Dynam.,* vol. 7, no. 4, 2012.

[11] M. Dumitriu and D. Stanica, “Effect of the Anti-Yaw Damper on Carbody Vertical Vibration and Ride Comfort of Railway Vehicles,” *Applied Sciences,* vol. 10, 2020.

[12] J. Chen, Y. Wu, X. He, L. Zhang and S. Dong, “Suspension parameter design of underframe equipment considering series stiffness of schock absorber,” *Advances in Mechanical Engineering,* vol. 12, 2020.

[13] G. Isacchi, F. Ripamonti and M. Corsi, “Innovative passive yaw damper to increase the stability and curve-taking performance of high-speed railway vehicles,” *Vehicle System Dynamics,* 2022.

[14] R. Greco and G. C. Marano, “Identification of parameters of Maxwell and Kelvin–Voigt generalized models for fluid viscous dampers,” *Journal of Vibration and Control,* vol. 21, no. 2, pp. 260-274, 2013.

[15] R. Greco, J. Avakian and G. C. Marano, “A comparative study on parameter identification of fluid viscous dampers with different models,” *Archive of Applied Mechanics,* vol. 84, no. 8, pp. 1117-1134, 2014.

[16] J. Guo, Z. Li and M. Zhang, “Parameter identification of the phenomenological model for magnetorheological fluid dampers using hierarchic enhanced particle swarm optimization,” *Journal of Mechanical Science and Technology,* vol. 35, no. 3, pp. 875-887, 2021.

[17] A. Rodríguez-Torres, M. López-Pacheco, J. Morales-Valdez, W. Yu and J. G. Díaz, “Robust Force Estimation for Magnetorheological Damper Based on Complex Value Convolutional Neural Network,” *J. Comput. Nonlinear Dynam,* vol. 17, no. 12, 2022.

[18] R. Rosmazi and M. Zamri, “Optimization of modified Bouc–Wen,” *Journal of Vibration and Control,* vol. 27, no. 17-18, pp. 1956-1967, 2020.

[19] B. A. Negash, W. You, J. Lee and K. Lee, “Parameter identification of Bouc-Wen model for Magnetorheological (MR) fluid Damper by a Novel Genetic Algorithm,” *Advances in Mechanical Engineering,* vol. 12, no. 8, pp. 1-12, 2020.

[20] X. Chen, L. Xu, S. Zhang, S. Zhao and K. Liu, “Parameter identification of the Bouc-Wen model for the magnetorheological damper using fireworks algorithm,” *Journal of Mechanical Science and Technology,* vol. 36, no. 5, pp. 2213-2224, 2022.

[21] X.-S. Yang, “Firefly Algorithms for Multimodal Optimization,” in *Proceedings of the 5th international conference on Stochastic algorithms: foundations and applications*, 2010.

[22] W. Teng, H. Shi, R. Luo, J. Zeng and C. Huang, "Improved nonlinear model of a yaw damper for simulating the dynamics of a high-speed train," *Proceedings of the Institution of Mechanical Engineers, Part F: Journal of Rail and Rapid Transit,* vol. 233, no. 7, pp. 651-665, 2018.

[23] A. Conde Mellado, E. Gomez and J. Vinolas, "Advances on railway yaw damper characterization exposed to small displacements," *International Journal of Heavy Vehicle Systems,* vol. 13, 2006.

[24] K. Knothe and S. Stichel, Rail Vehicle Dynamics, Springer, 2017.

[25] B. Bergander and W. Kunnes, "ERRI B176/DT 290: B176/3 benchmark problem, results and assessment: Technical report," European Rail Research Institute, 1993.

[26] G. Isacchi, F. Ripamonti, M. Corsi and T. Van Dongen, "A Smart Passive Yaw Damper for The Reduction of Lateral Contact Forces in Low-Radius Curved Tracks," in *WCCM-APCOM2022*, Yokohama, 2022.

[27] C. Huang and J. Zeng, "Dynamic behaviour of a high-speed train hydraulic yaw damper," *Vehicle System Dynamics,* vol. 56, no. 12, pp. 1922-1944, 2018.

Figure Captions List

Fig. 1	Damper dynamic model: the overall device composed by a main structure and two silent blocks.
Fig. 2	Block diagram of the overall tuning procedure of the damper model.
Fig. 3	Experimental test bench: (a) MTS® actuator to impose the reference strokes obtained from the multibody model to the yaw damper prototype. The actual damper force is measured by the load cell on the right side of the bench; (b) The SpeedGoat® Real Time Computer to acquire the output

signal (damper force) and to send the input signal (reference stroke) to the actuator through the MTS® Control Unit.

Fig.4 Damper stroke during the identification scenarios simulated with the multibody model ($x_{1,Id}$). (a) Straight track running at 250 km/h; (b) Low-speed negotiation of a sharp curve; (c) Switch negotiation.

Fig. 5 Damper stroke during the validation scenarios simulated with the multibody model ($x_{1,Val}$). (a) Straight track running at 250 km/h; (b) High-speed negotiation of large radius curve; (c) Low speed curve negotiation.

Fig. 6 Evolution of the mean fitness of the population.

Fig. 7 Comparison between the concentrated parameters of the initial and final population of damper models.

Fig. 8 Comparison of the nonlinear elastic and damping contributes between initial and final populations. The small amplitude region has been zoomed in both graphs.

Fig. 9 Comparison between experimental and optimal numerical force of the tested yaw damper. (a) Negotiation of sharp curve with radius 500 m. (b) Negotiation of large radius curve (6000 m) at 306 km/h. (c) Straight track high-speed running (250 km/h).

Fig. 10 Differences between experimental and optimal numerical force of the tested yaw damper. (a) Negotiation of sharp curve with radius 500 m. (b)

Negotiation of large radius curve (6000 m) at 306 km/h. (c) Straight track high-speed running (250 km/h).

Fig.11 Analysis of the nonlinear terms $F_{k,0}$ and $F_{c,0}$: the optimal terms (solid green line) are compared with a linear interpolation function (black dashed line) and with the even (yellow cross) and odd terms (red plus) of a 5th order polynomial function fitted on the data reported in table 2.

Table Caption List

Table 1 Summary of the main characteristics of identification and validation scenarios. The curvature and the rail cant are linearly variated along the clothoid transient segments.

Table 2 Optimal set of model parameters obtained after the implementation of the Firefly Algorithm.

Table 3 Numerical resume of the modelling performances of the proposed optimal damper model and the Maxwell linear model.

Figure 1

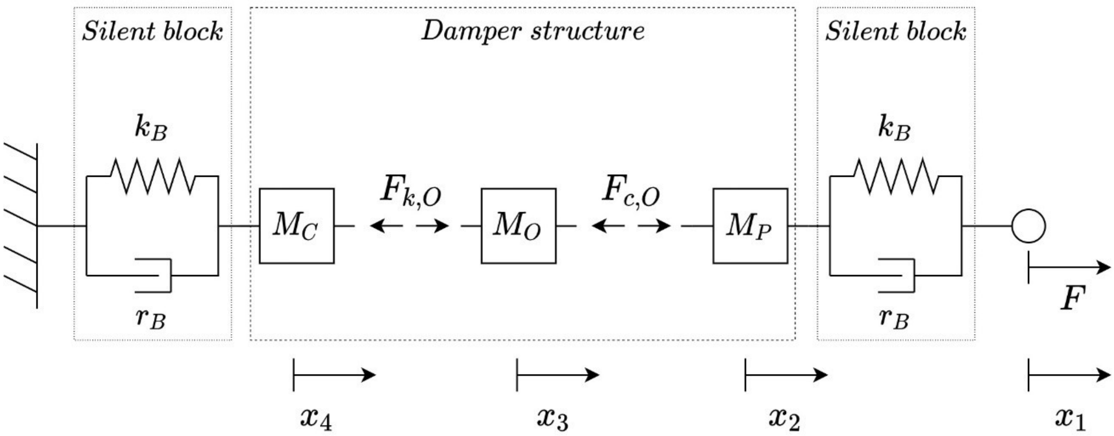
Silent block
Damper structure
Silent block
k_B
k_B
M_C
$F_{k,O}$
M_O
$F_{c,O}$
M_P
r_B
r_B
F
x_4
x_3
x_2
x_1

Figure 2

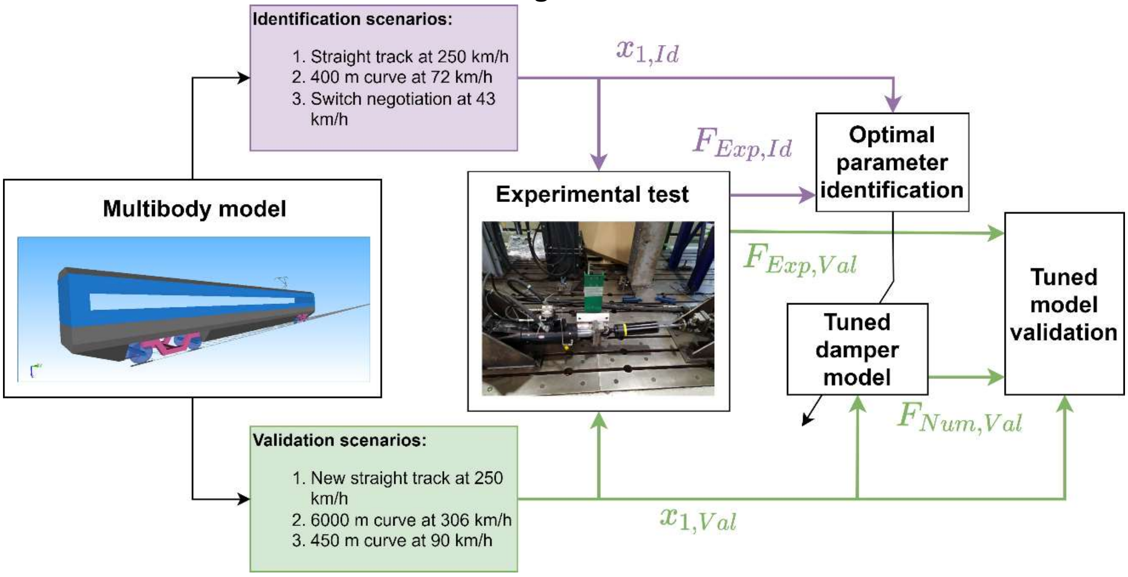
Identification scenarios:
1. Straight track at 250 km/h
2. 400 m curve at 72 km/h
3. Switch negotiation at 43 km/h
$x_{1,Id}$
$F_{Exp,Id}$
Optimal parameter identification
Multibody model
Experimental test
$F_{Exp,Val}$
Tuned model validation
Tuned damper model
$F_{Num,Val}$
Validation scenarios:
1. New straight track at 250 km/h
2. 6000 m curve at 306 km/h
3. 450 m curve at 90 km/h
$x_{1,Val}$

Figure 3

a)

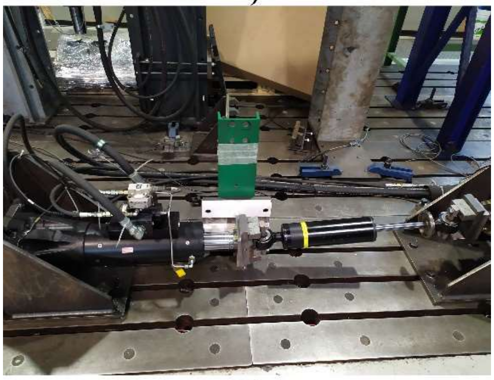

b)

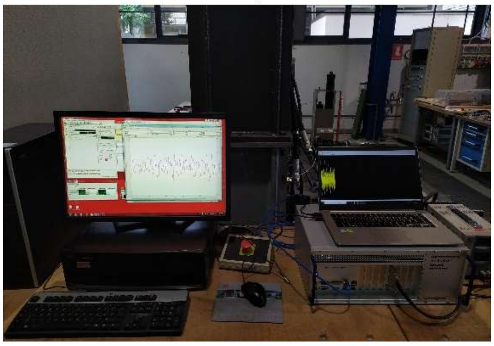

531 **Figure 4**

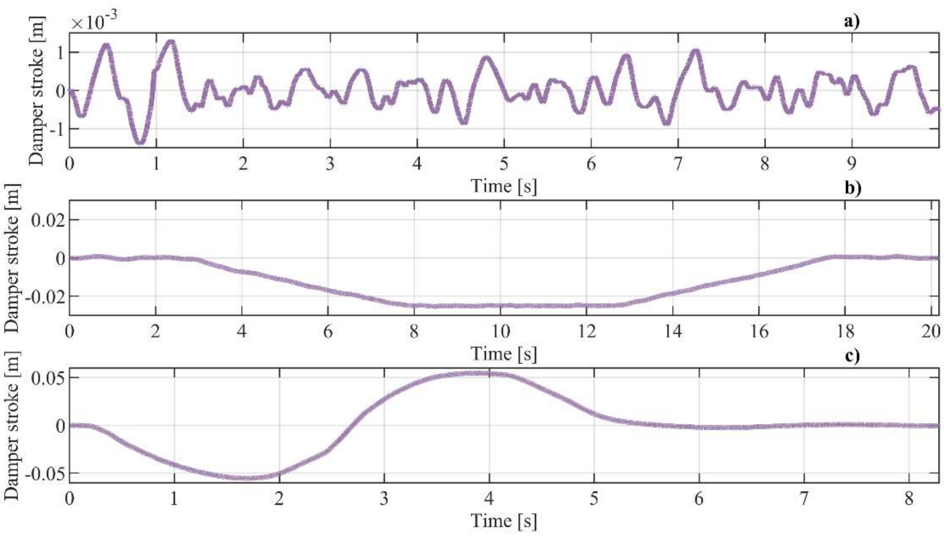

532
533

534 **Figure 5**

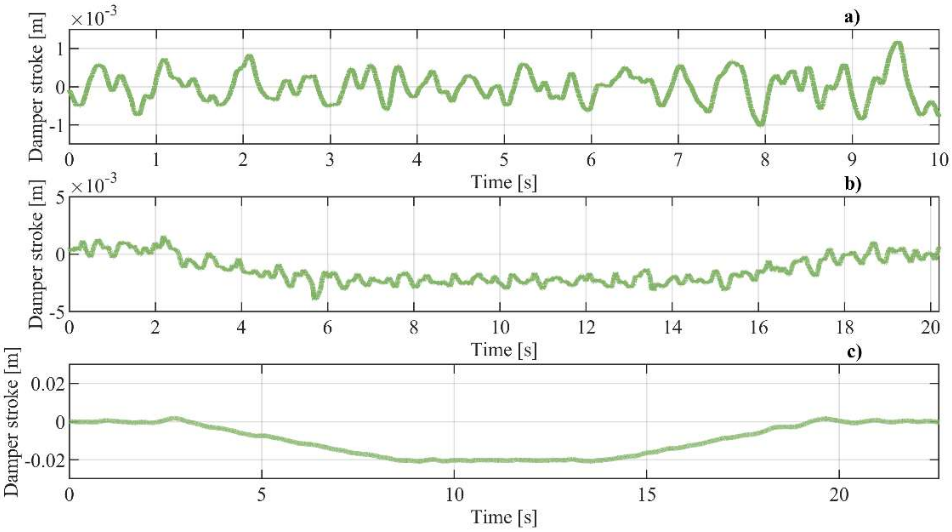

535
536

Figure 6

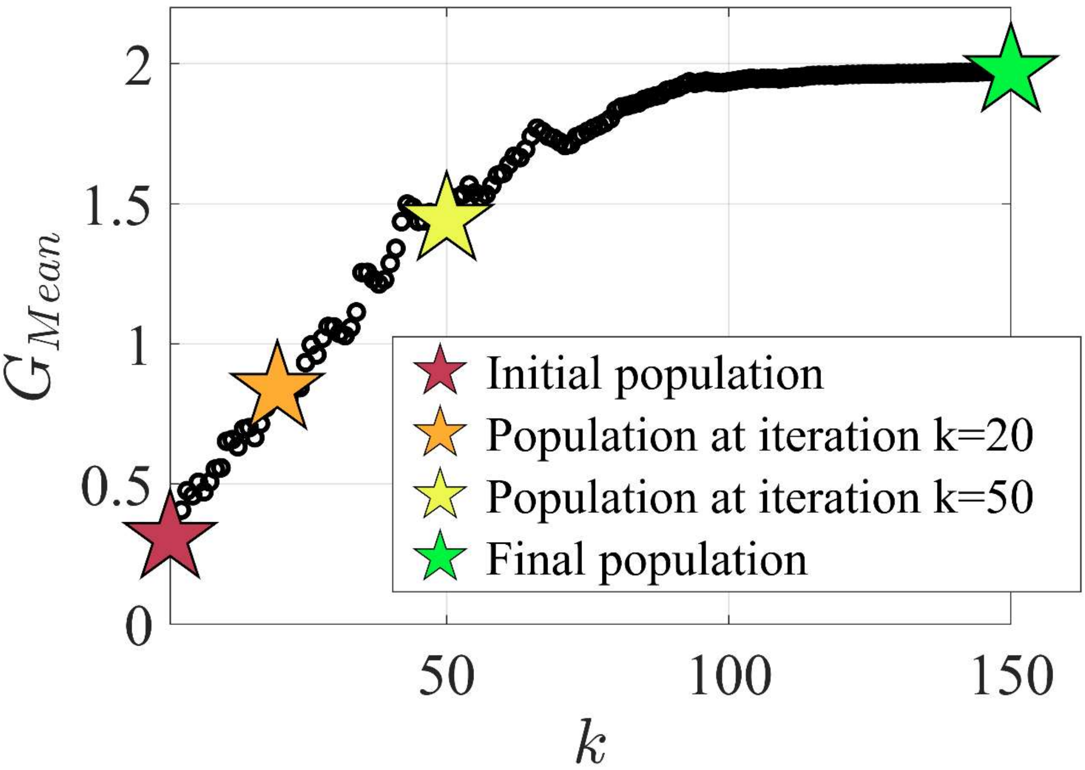
2
1.5
1
0.5
0
G_{Mean}
50
100
150
k
Initial population
Population at iteration k=20
Population at iteration k=50
Final population

540 **Figure 7**

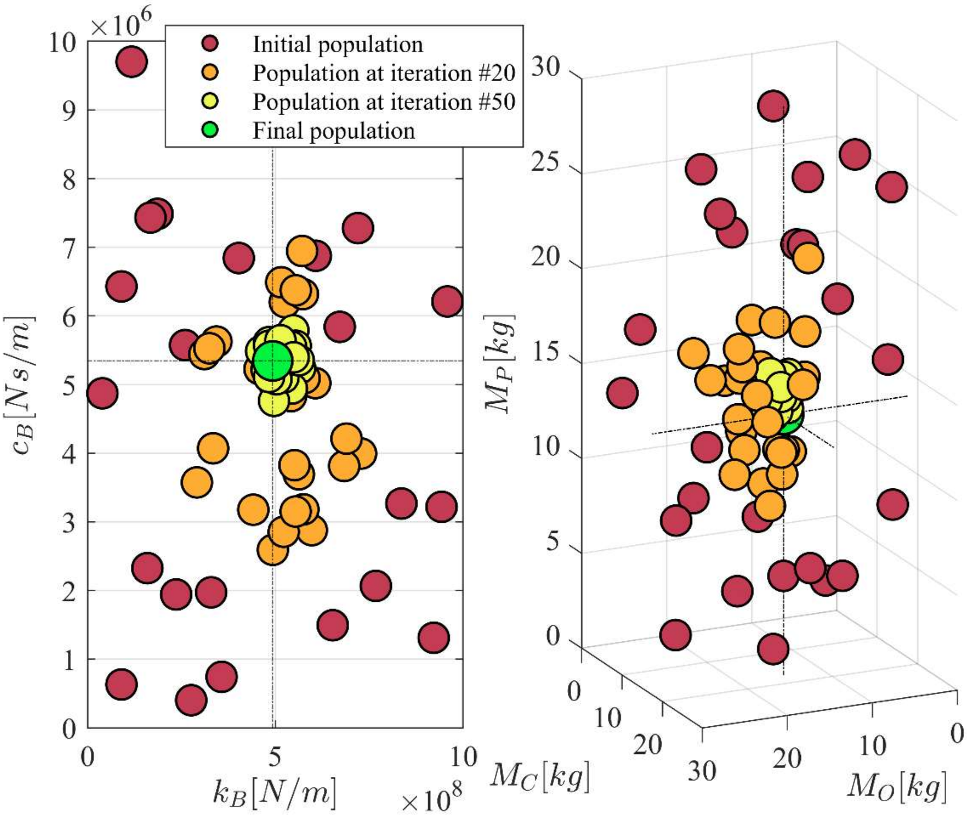

541
542

Figure 8

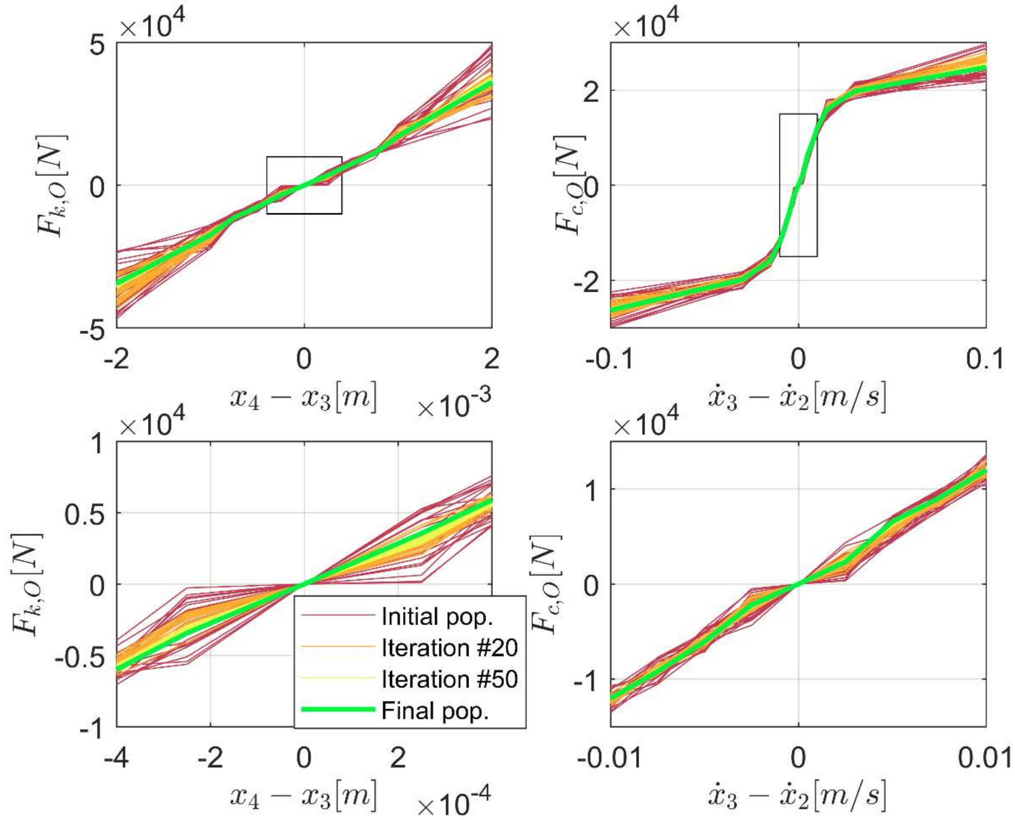
$\times 10^4$
$F_{k,O}[N]$
$x_4 - x_3[m]$
$\times 10^{-3}$
$F_{c,O}[N]$
$\dot{x}_3 - \dot{x}_2[m/s]$
$\times 10^{-4}$
Initial pop.
Iteration #20
Iteration #50
Final pop.

Figure 9

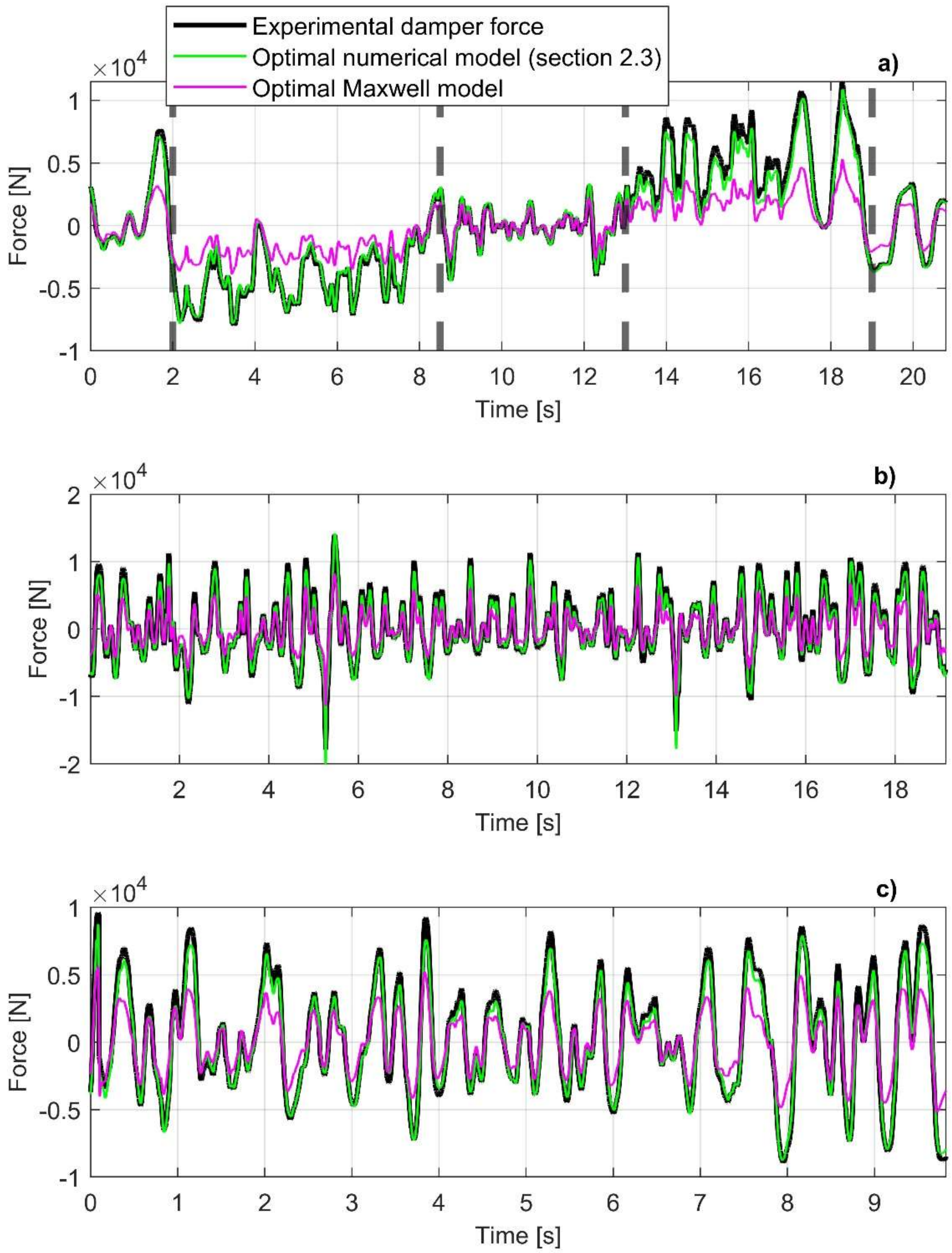
Experimental damper force
Optimal numerical model (section 2.3)
Optimal Maxwell model
a)
b)
c)
×10^4
Force [N]
Time [s]

554 **Figure 10**

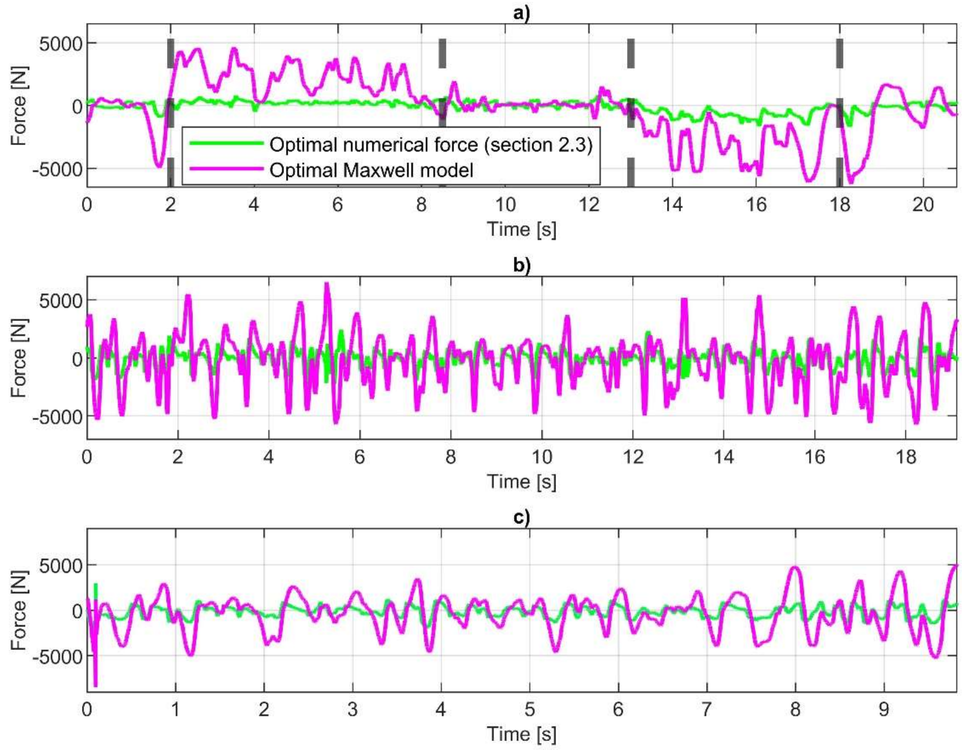

555
556
557

Figure 11

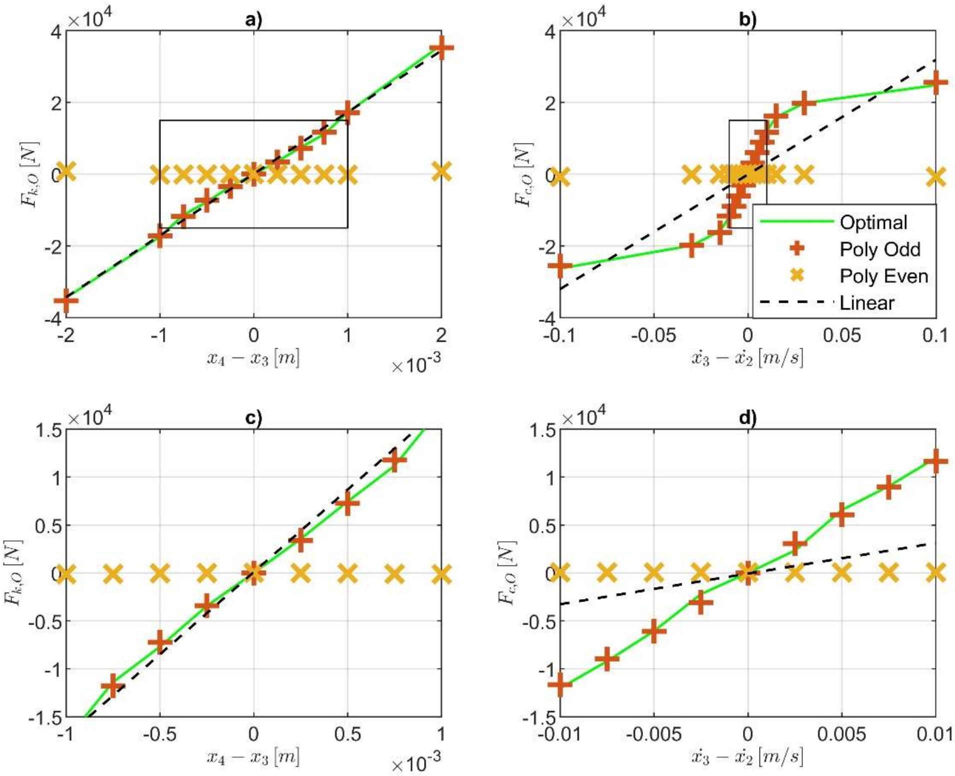
a)
b)
c)
d)
Optimal
Poly Odd
Poly Even
Linear
$F_{k,O}\,[N]$
$F_{c,O}\,[N]$
$x_4 - x_3\,[m]$
$\dot{x}_3 - \dot{x}_2\,[m/s]$
$\times 10^4$
$\times 10^{-3}$

Table1

Scenario	Vehicle speed [km/h]	Track irregularity	Track segments			
			#	**Type**	**Curve radius [m]**	**Rail cant [m]**
Identification 1	250 km/h	Present	1	Straight	∞	0
Identification 2	72 km/h	Present	1	Straight	∞	0
			2	Clothoid transient curve	From ∞ to 400	From 0 to 0.06
			3	Constant curve	400	0.06
			4	Clothoid transient curve	From 400 to ∞	From 0.06 to 0
			5	Straight	∞	0
Identification 3	43 km/h	Not present	1	Straight	∞	0
			2	Constant curve	190	0
			3	Straight	∞	0
			4	Constant curve	190	0
			5	Straight	∞	0
Validation 1	250 km/h	Present	1	Straight	∞	0
Validation 2	306 km/h	Present	1	Straight	∞	0
			2	Clothoid transient curve	From ∞ to 6000	From 0 to 0.09
			3	Constant curve	6000	0.09
			4	Clothoid transient curve	From 6000 to ∞	From 0.09 to 0
			5	Straight	∞	0
Validation 3	86 km/h	Present	1	Straight	∞	0
			2	Clothoid transient curve	From ∞ to 500	From 0 to 0.084
			3	Constant curve	500	0.084
			4	Clothoid transient curve	From 500 to ∞	From 0.084 to 0
			5	Straight	∞	0

Table 2

Parameter	Value	E.I.
M_O	16.5	[kg]
M_C	15.8	[kg]
M_P	17.3	[kg]
k_B	4.08e8	[N/m]
c_B	4.17e6	[Ns/m]
$[F_{k,O}]$	$[-34 \quad -17 \quad -11 \quad -7.7 \quad -3.4 \quad 0 \quad 3.6 \quad 7.5 \quad 11 \quad 17 \quad 36]$	[kN]
$[x_4 - x_3]$	$[-2 \quad -1 \quad -0.75 \quad -0.5 \quad -0.25 \quad 0 \quad 0.25 \quad 0.5 \quad 0.75 \quad 1 \quad 2]$	[mm]
$[F_{c,O}]$	$[-26 \quad -20 \quad -16 \quad -12 \quad -9.2 \quad -6.1 \quad -2.2 \quad 0 \quad 2.3 \quad 6.6 \quad 9.1 \quad 12 \quad 16 \quad 20 \quad 25]$	[kN]
$[\dot{x}_3 - \dot{x}_2]$	$[-100 \quad -30 \quad -15 \quad -10 \quad -7.5 \quad -5 \quad -2.5 \quad -0 \quad -2.5 \quad 5 \quad 7.5 \quad 10 \quad 15 \quad 30 \quad 100]$	[mm/s]

Table 3

	Maxwell model	**Proposed model**	**Error Percentage Variation**	**Maxwell model**	**Proposed model**	**Error Percentage Variation**
Index	$MSE = \frac{\sum_{i=1}^{N}\left(F_{Exp,i} - F_{Num,i}\right)^2}{N}$		$\frac{MSE_{Prop} - MSE_{Max}}{MSE_{Max}} 100$	$AME = \frac{\sum_{i=1}^{N}\left\|F_{Exp,i} - F_{Num,i}\right\|}{N}$		$\frac{AME_{Prop} - AME_{Max}}{AME_{Max}} 100$
Test 1	5.88e6 N^2	2.18e5 N^2	-96.3 %	1.80e3 N	346 N	-80.8 %
Test 2	5.05e6 N^2	5.32e5 N^2	-89.5 %	1.73e3 N	569 N	-67.1 %
Test 3	4.07e6 N^2	4.19e5 N^2	-89.7 %	1.55e3 N	526 N	-66.1 %